Primary ferrotoroidicity in antiferromagnets

P. Tolédano,[1] M. Ackermann,[2] L. Bohatý,[2] P. Becker,[2] T. Lorenz,[3] N. Leo,[4] and M. Fiebig[4]
[1]*Laboratoire de Systèmes Complexes, Université de Picardie, 80000 Amiens, France*
[2]*Institut für Kristallographie, Universität zu Köln, Greinstraße 6, 50939 Köln, Germany*
[3]*II. Physikalisches Institut, Universität zu Köln, Zülpicher Strasse 77, 50937 Köln, Germany*
[4]*Department of Materials, ETH Zürich, Vladimir-Prelog-Weg 4, 8093 Zurich, Switzerland*
(Received 25 June 2015; published 18 September 2015)

Antiferromagnetic ordering does not give rise to a measurable macroscopic symmetry-breaking order parameter such as the magnetization in a ferromagnet. An exception is the case of antiferromagnets with a vortexlike *toroidal* alignment of the magnetic moments in the unit cell because this gives rise to the formation of a spontaneous macroscopic toroidal moment which can be measured as a magnetoelectric effect. It is a long-standing question whether the toroidal moment is merely a side effect of the antiferromagnetic state or whether it can become the primary order parameter in a ferroic phase transition. Here we report the magnetoelectric properties of $LiFeSi_2O_6$ and show that they point to the role of the toroidal vector moment as the primary order parameter. Based on Landau theory we distinguish it from primary antiferromagnetic order. We thus justify the proposal that along with ferromagnets, ferroelectrics, and ferroelastics the ferrotoroidics constitute a new class of primary ferroics.

DOI: 10.1103/PhysRevB.92.094431 PACS number(s): 75.85.+t, 75.25.Dk, 75.30.Kz, 75.47.Lx

I. INTRODUCTION: TOROIDAL MOMENTS IN THE SOLID STATE

The existence of a ferroic state with a macroscopic spontaneous order parameter changing its sign under the application of space or time inversion has been the subject of many recent studies [1–5]. Such a state is formed by a periodic lattice of uniformly oriented toroidal moments $\mathbf{T} \propto \sum_{i=1}^{N} \mathbf{r}_i \times \mathbf{s}_i$ as illustrated in Fig. 1(b). Here $\mathbf{r}$ and $\mathbf{s}$ are the positions and spins of the N magnetic moments in a unit cell. The existence of toroidal moments is rooted in the toroidal part of the second order in the multipole expansion of the electromagnetic vector potential [6].

Thus far, toroidal moments have only been identified in antiferromagnetic structures. It therefore remains to be clarified if it is the toroidal moment or the antiferromagnetic coupling between the spins that drives the phase transition into the spin-ordered state. Only if the toroidal moment can act as the primary order parameter, and not merely as a side effect of antiferromagnetism, would "ferrotoroidicity" complement ferromagnetism, ferroelectricity, and ferroelasticity as a new, fully equivalent fourth form of primary ferroic order.

Symmetry considerations alone are insufficient for concluding whether the toroidal moment can be the driving mechanism for the transition to an antiferromagnetic state, since it has the same symmetry as the microscopic antiferromagnetic spin-wave order parameter. It is thus important to go beyond symmetry and find physical properties that allow one to distinguish the effects exerted by a primary toroidal order parameter from those exerted by a primary antiferromagnetic order parameter. An obvious choice is the magnetoelectric effect which was used previously to couple to the spontaneous toroidal moment of a compound and orient it in a controlled, hysteretic way [5]. The linear magnetoelectric effect denotes induction of a magnetization by an electric field ($M_k \propto \alpha_{ik} E_i$) or of an electric polarization by a magnetic field ($P_i \propto \alpha_{ik} H_k$). Spontaneous toroidal moments are found in antiferromagnetic structures displaying an antisymmetric part, i.e., $\alpha_{ik}^{\text{asym}} = -\alpha_{ki}^{\text{asym}}$, of the linear magnetoelectric effect [7].

Here we show that the magnetoelectric properties disclosed in the pyroxene compound $LiFeSi_2O_6$ [8–12] can be associated with a primary ferrotoroidic order parameter. We measure all the components α_{ik} of the magnetoelectric tensor and discuss the magnetic symmetry derived from it. Based on Landau theory we show that primary ferrotoroidic order can explain the resulting symmetry whereas primary antiferromagnetic order cannot.

The toroidal moment $\mathbf{T}$ is a macroscopic polar vector antisymmetric under time reversal [1–7]. Therefore, candidate compounds for ferrotoroidic order have to fulfill the necessary conditions that the transition wave vector is at the center of the paramagnetic Brillouin zone ($\mathbf{q} = 0$), and that the magnetic symmetry of the antiferromagnetic state violates space- and time-inversion symmetry and permits toroidal components [7]. These conditions are realized by the low-temperature magnetic transition occurring in $LiFeSi_2O_6$ [10–12]. The space group $C2/c1'$ of the crystal at room temperature transforms to $P2_1/c1'$ at a structural transition at 230 K [10]. At 23.2 K the monoclinic unit cell with lattice dimensions $a = 9.651$ Å, $b = 8.7057$ Å, $c = 5.2790$ Å, and $\beta = 109.929°$ contains four Fe^{3+} ions, the positions of which are given in Figs. 1(a) and 1(b). Neutron diffraction [10–12] shows a transition to a unit-cell preserving ($\mathbf{q} = 0$) antiferromagnetic state at the Néel temperature $T_N = 18$ K. The magnetic phase is identified as having a monoclinic magnetic space group $P2_1/c'$ which allows a linear magnetoelectric effect [8]. Note that all our measurements and their discussion are based on a Cartesian reference system with unit axes $\mathbf{e}_x$, $\mathbf{e}_y$, and $\mathbf{e}_z$, where $\mathbf{e}_y$ and $\mathbf{e}_z$ are running parallel to the crystallographic b and c axis, respectively, and $\mathbf{e}_x = \mathbf{e}_y \times \mathbf{e}_z$. The transformation matrix between the crystallographic system $\{\mathbf{a},\mathbf{b},\mathbf{c}\}$ and the Cartesian system $\{\mathbf{e}_x,\mathbf{e}_y,\mathbf{e}_z\}$ is given by

$$\mathbf{r} = A\mathbf{a} + B\mathbf{b} + C\mathbf{c} \tag{1}$$

$$= Aa\sin\beta\,\mathbf{e}_x + Bb\,\mathbf{e}_y + (Aa\cos\beta + Cc)\,\mathbf{e}_z \tag{2}$$

with $\beta = \angle(\mathbf{a},\mathbf{c}) \neq 90°$. As we see, $\mathbf{b} \parallel \mathbf{e}_y$ denotes the twofold symmetry axis and the ac mirror plane transforms into

 ©2015 American Physical Society

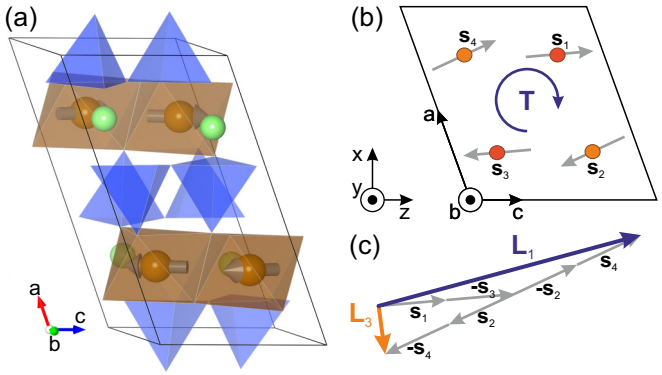

FIG. 1. (Color online) Primary ferrotoroidic order in $LiFeSi_2O_6$. (a) View of the magnetic unit cell with edge-sharing chains of $Fe^{3+}O_6$ octahedra (brown), SiO_4 tetrahedra (blue), and Li ions (green). Gray arrows depict the Fe^{3+} magnetic moments [11,12]. (b) Magnetic order within the ac, respectively xz, plane with spins $\mathbf{s}_i$ ($i = 1 \ldots 4$). Spins on sites 1 and 3, respectively 2 and 4, are antiparallel, while the in-chain pairs (1-4, 2-3) are mainly coupled ferromagnetically. Due to the vortexlike arrangement a toroidal moment $\mathbf{T}$ emerges along the $\mathbf{b} \parallel \mathbf{e}_y$ direction (blue circle). (c) Depiction of the spin sums contributing to the antiferromagnetic exchange interaction. We have $\mathbf{L}_1 = \mathbf{s}_1 - \mathbf{s}_2 - \mathbf{s}_3 + \mathbf{s}_4$ and $\mathbf{L}_3 = \mathbf{s}_1 + \mathbf{s}_2 - \mathbf{s}_3 - \mathbf{s}_4$. The leading exchange contribution is given by a term $\propto (\mathbf{L}_1 \cdot \mathbf{L}_3)^2$ which is suppressed because of the approximate relation $\mathbf{L}_1 \perp \mathbf{L}_3$.

the xz mirror plane. In Cartesian coordinates, the nonzero components of the linear magnetoelectric tensor in the $P2_1/c'$ phase are [13] α_{xx}, α_{yy}, α_{zz}, α_{xz}, and α_{zx}.

II. LINEAR MAGNETOELECTRIC EFFECT

Figure 2 shows the temperature dependence of the linear magnetoelectric effect in $LiFeSi_2O_6$. It was measured as magnetic-field-induced electric polarization for all nine components α_{ik}. Because of the large difference between the components we took particular care to minimize errors such as sample misalignments with respect to the applied magnetic fields or a possible mismatch of the sample electrodes, which could easily admix intensity from large onto small or zero components of the tensor $[\alpha_{ik}]$. The sample misalignment with respect to the applied magnetic fields was minimized to about 1°. In order to assure well-matched electrode areas the sample surfaces were completely vapor metallized with silver electrodes. Furthermore, the influence of nonidentical electrodes on the pyroelectric current measurements was systematically investigated (for more details see Ref. [14]).

In almost all cases the magnetoelectric domains in simultaneously applied magnetic and electric fields could be completely inverted by inverting either the magnetic or the electric field. Either reversal leads to a sign change of the corresponding magnetoelectric tensor components. We find that *all components except* α_{yy} are different from zero, which is an unexpected result. Several components not permitted in the previously established magnetic space group $P2_1/c'$ are observed, which points to a lower, triclinic, symmetry. In contrast, the zero-ness of α_{yy} is not required by symmetry. For a magnetic field applied along $\mathbf{e}_y$ no magnetic-field-induced pyroelectric current along $\mathbf{e}_y$ could be resolved from the background noise of about ± 20 fA. As an additional irregularity, a sharp drop in the temperature dependence of P_y for $\mathbf{H} \parallel \mathbf{e}_z$ [Fig. 2(f)] occurring near 8 K for $\mu_0 H > 10$ T points to an additional symmetry-changing magnetic phase transition.

III. OPTICAL BIREFRINGENCE

In order to verify the triclinicity of the magnetic phase in the absence of an applied magnetic field the linear optical properties were measured by polarization microscopy between room temperature and 4 K. We did this by investigating the orientational dispersion of the optical indicatrix [15]. For monoclinic crystals, its dispersion is restricted to pure rotations around the $\mathbf{e}_y$ axis by the symmetries $2 \parallel \mathbf{e}_y$ and $m \perp \mathbf{e}_y$ whereas there is no such restriction for lower (triclinic) symmetries. For our investigation we used two polished crystal plates, one with faces perpendicular to $\mathbf{e}_x$ with a thickness of 86 μm and one with its faces perpendicular to the $\mathbf{e}_z$ axis and a thickness of 303 μm. On the former we detected a rotation of the principal axes of the indicatrix out of the xz plane below T_N. This was done by measuring the inclination angle θ of extinction between crossed polarizers with respect to the $\mathbf{e}_y$ axis in orthoscopic observation. As required in the monoclinic phase, θ remained at 0° above T_N. Below T_N, however, it augmented to a value of $\approx 2^\circ$ at 4 K as shown in Fig. 3.

In an additional test we verified the orientational dispersion of the optical axes. In optically biaxial $LiFeSi_2O_6$ the two optical axes lie in the xz plane. One of them is seen with the $\mathbf{e}_z$-cut sample in conoscopic observation. The orientational dispersion of this optical axis within the xz plane above T_N changes to an out-of-plane orientational dispersion below T_N, which is symmetry forbidden in monoclinic crystals. The rotation of the optical axis plane of the indicatrix out of the xz plane of the crystal is another confirmation that in contrast to the previously proposed monoclinic symmetry [9,12] the magnetic phase of $LiFeSi_2O_6$ below T_N is actually triclinic.

IV. SYMMETRY ANALYSIS

The paramagnetic space group $P2_1/c1'$ at $\mathbf{q} = 0$ yields the four monoclinic magnetic space groups $P2_1/c$ (Γ_1^+), $P2_1'/c'$ (Γ_2^+), $P2_1/c'$ (Γ_1^-), and $P2_1'/c$ (Γ_2^-), here with the corresponding one-dimensional irreducible representations given in brackets (see Table I) [16]. Their subsequent activation can induce a variety of magnetic phases as depicted in Fig. 4. The transition of $LiFeSi_2O_6$ to the triclinic phase, as concluded from the magnetoelectric and the birefringence measurements, requires the simultaneous condensation of more than one irreducible order parameter. According to Fig. 4, only the group $P\bar{1}'$ induced by $\Gamma_1^- + \Gamma_2^-$ can explain the observed linear magnetoelectric effect in $LiFeSi_2O_6$.

A. Analysis in terms of magnetic spin modes

The correspondence between the symmetry of the magnetic irreducible representation and sums of the local moments can be found as follows. We construct a reducible representation from the permutation of the magnetic moments on the local sites by application of the symmetry operations of the crystallographic $P2_1/c1'$ parent group. This leads to a

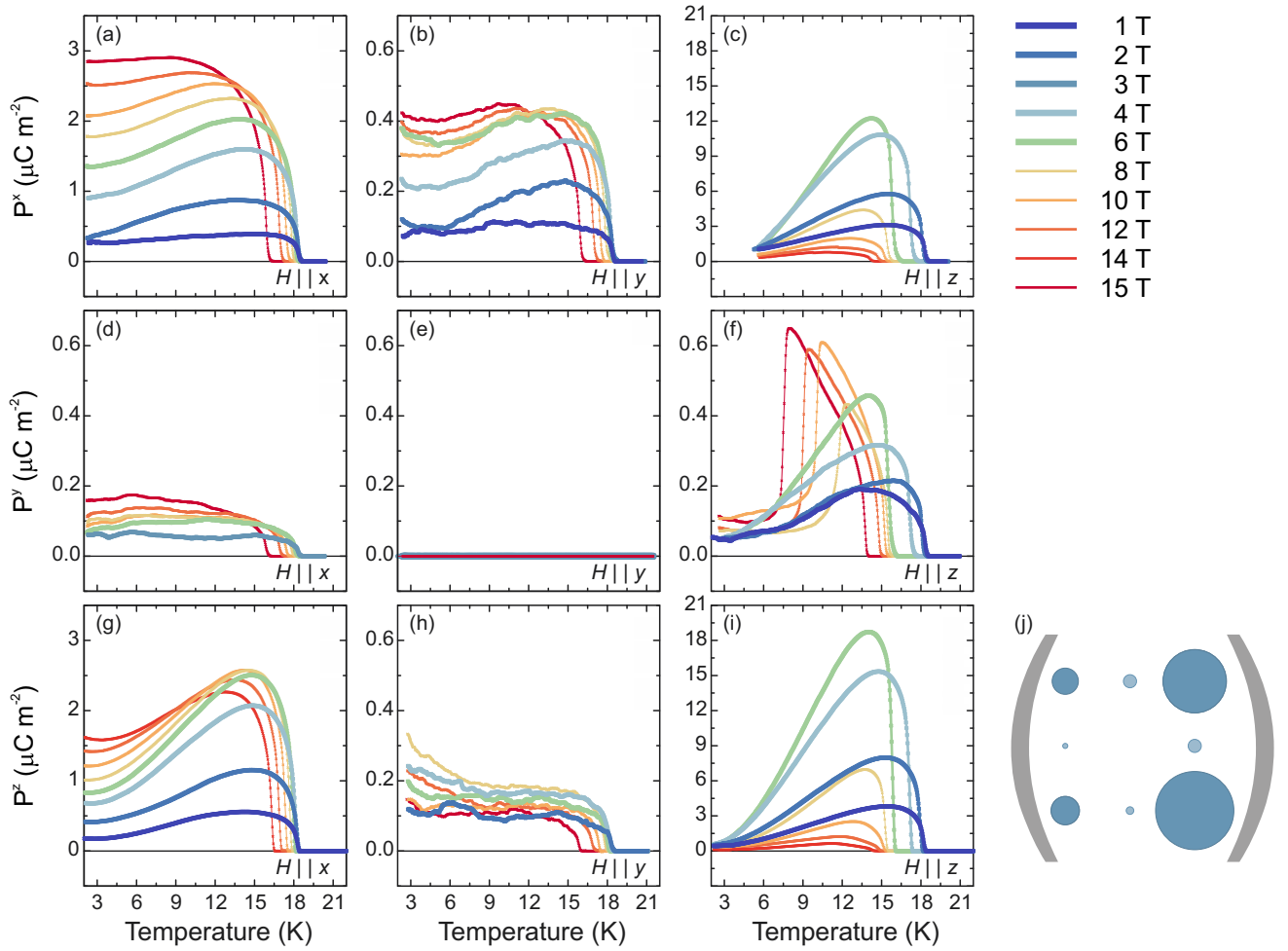

FIG. 2. (Color online) Linear magnetoelectric effect in $LiFeSi_2O_6$. (a)–(i) Temperature dependence of the electric polarization P^x, P^y, P^z (top to bottom) for magnetic fields $\mu_0 H$ applied parallel to the $\mathbf{e}_x$, $\mathbf{e}_y$, or $\mathbf{e}_z$ axis (left to right). (j) Relative magnitude (proportional to circle area) of the magnetoelectric polarization at 14 K and 3 T. Γ_1^-- and Γ_2^--related contributions are bright and dark gray, respectively.

12-dimensional representation, as summarized in Table II, and four possible sums of the magnetic moments on the iron sites, namely,

$$\mathbf{M} = \mathbf{s}_1 + \mathbf{s}_2 + \mathbf{s}_3 + \mathbf{s}_4, \tag{3}$$

$$\mathbf{L}_1 = \mathbf{s}_1 - \mathbf{s}_2 - \mathbf{s}_3 + \mathbf{s}_4, \tag{4}$$

$$\mathbf{L}_2 = \mathbf{s}_1 - \mathbf{s}_2 + \mathbf{s}_3 - \mathbf{s}_4, \tag{5}$$

$$\mathbf{L}_3 = \mathbf{s}_1 + \mathbf{s}_2 - \mathbf{s}_3 - \mathbf{s}_4, \tag{6}$$

where the spin-density vectors in Eqs. (3)–(6) represent the four magnetic order parameters. By comparison of the transformation of the magnetic moments on the different sites (or using group-theoretical projection methods [17]) these sums of spins can be associated with the transformation behavior of the magnetic irreducible representations $\Gamma_i^{\pm}$, as listed in the last column of Table I. We thus see that Γ_1^- and Γ_2^- are spanned, respectively, by the spin-density-wave projections (L_1^x, L_3^y, L_1^z) and (L_3^x, L_1^y, L_3^z). In turn, the microscopic modes transforming like the irreducible representations Γ_1^+ and Γ_2^+ are inactive. The associated zero-ness of the modes $\mathbf{M}$ and $\mathbf{L}_2$ yields six relations between the spins in the magnetic unit cell, which are $\mathbf{s}_1 = -\mathbf{s}_3$ and $\mathbf{s}_2 = -\mathbf{s}_4$ in correspondence with the spin structure shown in Fig. 1(b). Those moments on sites related by the spatial inversion operation are strictly coupled antiferromagnetically, and the discussion of the magnetic structure can be simplified by considering only the Fe^{3+} moments within the edge-sharing chains along the c direction.

Note that the $P2_1/c'$ symmetry proposed in earlier investigations of $LiFeSi_2O_6$ corresponds to the presence of the Γ_1^- mode only. In this case the in-chain moments ($\mathbf{s}_1$ and $\mathbf{s}_4$, and $\mathbf{s}_2$ and $\mathbf{s}_3$, respectively) are coupled ferromagnetically along the x and z direction, and antiferromagnetically along the y direction so that $s_4^{x,z} = s_1^{x,z}$ and $s_4^y = -s_1^y$. With the additional Γ_2^- mode leading to the triclinic $P\bar{1}'$ symmetry, the magnetic moments $s_{1,4}^{x,z}$ are no longer exactly parallel and in addition the in-chain moment along y has a ferromagnetic contribution.

B. Analysis in terms of toroidal moment

As an alternative to an association to spin waves, symmetry permits one to express the order parameters in terms of the components of a macroscopic toroidal vector $\mathbf{T}$. Then, Γ_1^- and Γ_2^- have the symmetry of the components T^y and

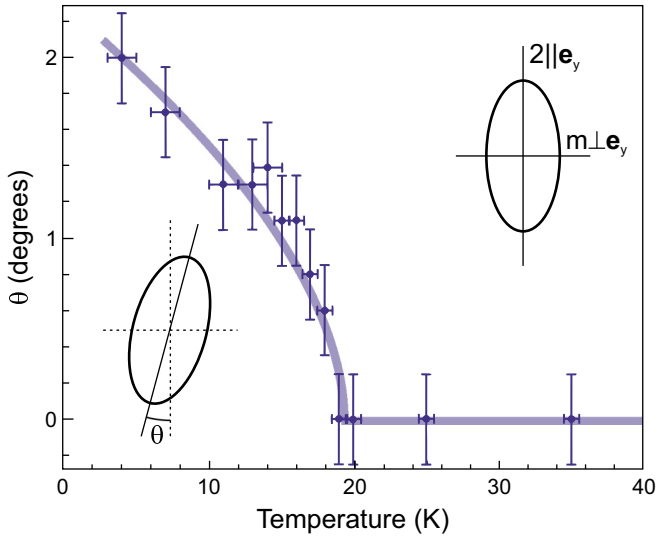

FIG. 3. (Color online) Measured inclination angle of the extinction angle θ relative to the $\mathbf{e}_y$ axis of a $LiFeSi_2O_6$ (100) plate, using an incident wave with wave normal along $\mathbf{e}_x$. A polarizing microscope with crossed polarizers was used for the observation. Above $T_N = 18$ K, we get $\theta = 0°$ in accordance with monoclinic symmetry. Below T_N the rotational degree of freedom expressed by $\theta \neq 0°$ indicates the loss of the monoclinic symmetry elements $2 \parallel \mathbf{e}_y$, $m \perp \mathbf{e}_y$ and, hence, a triclinic symmetry of the crystal. The line is a guide to the eye.

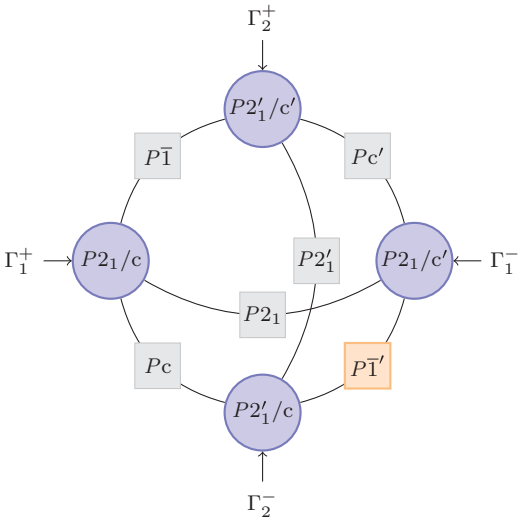

FIG. 4. (Color online) Possible magnetic space groups obtained from the $P2_1/c1'$ parent group by activation of irreducible representations Γ_i defined in Table I. A single active representation can induce the phases highlighted by blue circles. The magnetic space groups in rectangles are acquired if two representations are nonzero. The only phase in agreement with the observed magnetoelectric effect in $LiFeSi_2O_6$ is the space group $P\bar{1}'$ (orange square). It requires both Γ_1^- and Γ_2^- to be active.

$T^{x,z}$ of $\mathbf{T}$, respectively. Here, $\mathbf{T}$ corresponds to the toroidal moment defined by $\mathbf{T} = \frac{1}{2V}\Delta\mathbf{r}_i \times \mathbf{s}_i$, with unit-cell volume V, ionic displacements $\Delta\mathbf{r}_i$, and magnetic moments $\mathbf{s}_i$ [2]. The displacements $\Delta\mathbf{r}_i$ are calculated with respect to the room-temperature phase with symmetry $C2/c1'$. For the magnetic structure in $LiFeSi_2O_6$ this formula yields

$$\mathbf{T} = \frac{1}{V}\begin{pmatrix} \Delta r^y\left(s_1^z - s_4^z\right) - \Delta r^z\left(s_1^y + s_4^y\right) \\ \Delta r^z\left(s_1^x + s_4^x\right) - \Delta r^x\left(s_1^z + s_4^z\right) \\ \Delta r^x\left(s_1^y + s_4^y\right) - \Delta r^y\left(s_1^x - s_4^x\right) \end{pmatrix}. \quad (7)$$

Symmetry considerations alone do not allow us to discriminate which of the two order parameters, antiferromagnetic $\mathbf{L}_i$ or toroidal $\mathbf{T}$, represents the primary symmetry-breaking transition mechanism in $LiFeSi_2O_6$. Regarding their physical origin, however, the interactions giving rise to the toroidal moment and to the spin-density waves are different. In particular, the macroscopic toroidal moment results from a variety of contributions, i.e., $\mathbf{T} = \mathbf{T}_{\text{spin}} + \mathbf{T}_{\text{orb}} + \mathbf{T}_{\text{other}}$. Here $\mathbf{T}_{\text{spin}}$ represents the contribution of localized spins as in Fig. 1(b) forming the spin-density waves involved in the formation of toroidal moments. $\mathbf{T}_{\text{orb}}$ is the contribution of the orbital moments of the electron current density to the toroidal moment, which is several orders of magnitude smaller than the spin contribution [18]. $\mathbf{T}_{\text{other}}$ are other possible contributions to the toroidal moment as, for example, higher-order toroidal moments in the multipole expansion of the electromagnetic vector potential. Therefore, although both the spin wave and the toroidal order parameter contribute to the internal magnetic field and to the resulting magnetoelectric effect, they can result from different interactions. The specific features of these effects should allow us to determine the actual symmetry-breaking order parameter that is the primary driving force behind the transition into the triclinic magnetic ground state below T_N. In the following, we will show that a primary antiferromagnetic spin-density-wave order parameter is unlikely whereas the toroidal moment as the primary order parameter yields a consistent description of the transition in $LiFeSi_2O_6$.

TABLE I. Magnetic irreducible representations of the monoclinic space group $P2_1/c1'$ at the center of the Brillouin zone ($\mathbf{q} = 0$). $1'$ denotes the time-reversal operator. The physical basis functions, given in the last column, transform according to the respective representations. Here, $\mathbf{H}$ and $\mathbf{T}$ denote the macroscopic magnetic field and the toroidal moment, respectively. $\mathbf{M}$ and $\mathbf{L}_{1,2,3}$ correspond to microscopic spin-density waves defined in Eqs. (3)–(6).

	$1\|000$	$2_y\|0\frac{1}{2}\frac{1}{2}$	$\bar{1}\|000$	$m_y\|0\frac{1}{2}\frac{1}{2}$	$1'$	Basis functions	
Γ_1^+	1	1	1	1	−1	H^y	$L_2^{x,z}, M^y$
Γ_2^+	1	−1	1	−1	−1	$H^{x,z}$	$M^{x,z}, L_2^y$
Γ_1^-	1	1	−1	−1	−1	T^y	$L_1^{x,z}, L_3^y$
Γ_2^-	1	−1	−1	1	−1	$T^{x,z}$	$L_3^{x,z}, L_1^y$

V. PHASE TRANSITION MECHANISMS

The coefficients of the magnetoelectric tensor in Fig. 2 were measured by recording the electric polarization current induced at different values of the magnetic field. For the triclinic symmetry $P\bar{1}'$ all nine components of the magnetoelectric tensor can be nonzero. We note, however, that the magnetoelectric coefficients α_{ik} associated to the representations Γ_1^- and Γ_2^- differ substantially in magnitude according to Fig. 2(j).

TABLE II. Reducible representation for determination of magnetic modes of the Fe^{3+} moments. The ions occupy sites with the positions $1-(x,y,z)$, $2-(1-x,y+\frac{1}{2},\frac{1}{2}-z)$, $3-(1-x,1-y,1-z)$, and $4-(x,\frac{1}{2}-y,z+\frac{1}{2})$ (see Fig. 1). Matrices in the first row give the permutation of these sites with the space-group symmetry elements; the second row lists the transformation behavior of the local spins $\mathbf{s}_{1,2,3,4}$ under the symmetry operations.

	$1\|000$	$2_y\|0\frac{1}{2}\frac{1}{2}$	$\bar{1}\|000$	$m_y\|0\frac{1}{2}\frac{1}{2}$
Sites	$\begin{pmatrix}\blacksquare & & & \\ & \blacksquare & & \\ & & \blacksquare & \\ & & & \blacksquare\end{pmatrix}$	$\begin{pmatrix} & \blacksquare & & \\ \blacksquare & & & \\ & & & \blacksquare \\ & & \blacksquare & \end{pmatrix}$	$\begin{pmatrix} & & \blacksquare & \\ & & & \blacksquare \\ \blacksquare & & & \\ & \blacksquare & & \end{pmatrix}$	$\begin{pmatrix} & & & \blacksquare \\ & & \blacksquare & \\ & \blacksquare & & \\ \blacksquare & & & \end{pmatrix}$
Spin	$\begin{pmatrix}s^x\\ s^y\\ s^z\end{pmatrix}$	$\begin{pmatrix}-s^x\\ s^y\\ -s^z\end{pmatrix}$	$\begin{pmatrix}s^x\\ s^y\\ s^z\end{pmatrix}$	$\begin{pmatrix}-s^x\\ s^y\\ -s^z\end{pmatrix}$

For the coefficients coinciding with a $P2_1/c'$ (Γ_1^-) symmetry (i.e., α_{xx}, α_{yy}, α_{zz}, α_{xz}, α_{zx}) and the toroidal component T^y one has $P^x(H^x)=1.30$, $P^z(H^x)=1.51$, $P^x(H^z)=7.58$, $P^z(H^z)=11.53$ in units of $\mu\,\mathrm{Cm}^{-2}$ at 14 K and $\mu_0 H=3$ T. In contrast, the coefficients associated with a $P2_1'/c$ (Γ_2^-) symmetry (i.e., α_{yx}, α_{zy}, α_{xy}, α_{yz}) and the toroidal components $T^{x,z}$ yield $P^y(H^x)=0.05$, $P^z(H^y)=0.11$, $P^x(H^y)=0.33$, $P^y(H^z)=0.33$. The difference in magnitude between the two sets and the outstanding zero-ness of $P_y(H_y)$ suggests an interplay of two mechanisms.

(i) A *triggering mechanism* at T_N in which the primary toroidal order parameter T^y allowed by the $P2_1/c'$ symmetry triggers the onset of secondary order-parameter components T^x and T^z reduces the symmetry further to $P\bar{1}'$ [19]. Such a triggering mechanism is expressed by the symmetry-allowed biquadratic coupling between the toroidal moment components in a contribution $\delta(T^y)^2(T^{x,z})^2$ to the free energy. It has been shown [19,20] that such a mechanism, illustrated by the phase diagram of Fig. 5(a), can occur as a first-order phase transition if the coefficient for the coupling of the order parameters, here δ, is negative and sufficiently large. In fact, a marked decrease of the b and c lattice parameters at T_N by about 0.045% was reported in neutron-diffraction experiments [10]. These data, as well as capacitance dilatometry and specific-heat measurements, do not identify a discontinuity or hysteresis at T_N. This points to a weak first-order character of the phase transition. Note that the induced, secondary nature of $T^{x,z}$ in relation to the triggering, primary nature of T^y is further supported by $\alpha_{ij}(T^{x,z}) \ll \alpha_{ij}(T^y)$.

(ii) A *deactivation mechanism* under an applied magnetic field H^y serves as an explanation for the zero-ness of α_{yy}. The field H^y quenches the Γ_1^- mode and leaves the Γ_2^- mode, thereby shifting the symmetry from triclinic $P\bar{1}'$ to monoclinic Pc [Fig. 5(d)]. For this symmetry, we have α_{xy}, $\alpha_{zy}\neq 0$, and $\alpha_{yy}=0$ so that we get $P^{x,z}\neq 0$, but $P^y=0$ in the applied field H^y in agreement with the measurements shown Fig. 2. In terms of the order parameters, T^y is deactivated by the magnetic field H^y whereas $T^{x,z}$ remain active. Such a deactivation mechanism is also supported by the small values found for α_{xy} and α_{zy}, which indicates that these components are exclusively related to the triggered, secondary-order-parameter components $T^{x,z}$, as discussed above.

Although permitted by symmetry, the origin of the biquadratic coupling between the components T^y and $T^{x,z}$ of the toroidal moment vector at the microscopic level is unclear. A possible way to explain it is to associate T^y and $T^{x,z}$ to the spin and orbital part of the toroidal moment, respectively. The contribution of the orbital moments of the electron current density to the internal magnetic field is much smaller than that of the spins [18], which would explain the order of magnitude

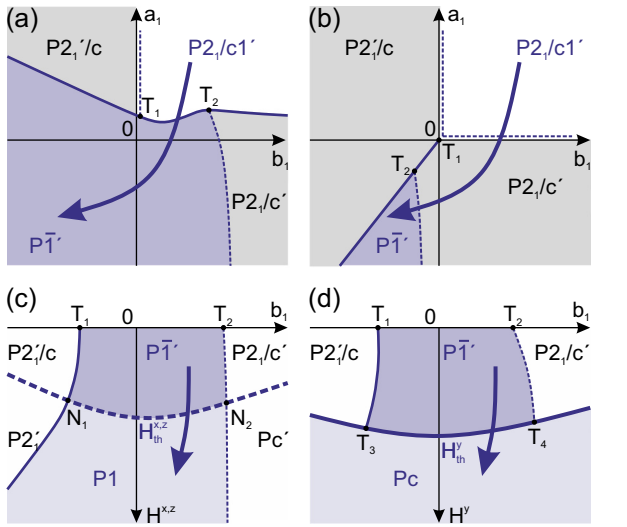

FIG. 5. (Color online) Schematic phase diagrams associated with the free-energy $F=a_1(T^y)^2+a_2(T^y)^4+b_1(T^{x,z})^2+b_2(T^{x,z})^4+b_3(T^{x,z})^6+\delta(T^y)^2(T^{x,z})^2-\mathbf{H}^2(\delta_1(T^{x,z})^2+\delta_2(T^y)^2+\delta_3T^xT^z)$. Hatched and solid curves represent second- and first-order transitions curves. T_1 to T_4 are triple points. N_1 and N_2 are four-phase points. Arrows show the thermodynamic paths assumed in our description. (a),(b) Phase diagrams without applied magnetic fields ($\mathbf{H}=0$). (a) Phase diagram for a strong negative δ coupling promoting the triggering mechanism, so that the $P\bar{1}'$ phase is reached in a single step [$\delta<-2(|a_2|b_2)^{0.5}$, $a_2<0$]. (b) Phase diagram for weak coupling of the antiferromagnetic order parameters [$\delta>2(|a_2|b_2)^{0.5}$, $a_2<0$]. Now the $P\bar{1}'$ phase is reached by two successive phase transitions across the region of stability of the $P2_1/c'$ phase. (c),(d) Projections of the field-induced phase diagrams on the $(b_1,H^{x,z})$ and (b_1,H^y) planes for strong coupling of the order parameters. In (c) the $P1$ phase is reached continuously above threshold fields H^x_{th} and H^z_{th}. In (d) the threshold field H^y_{th} decouples the T^y order parameter and the $P\bar{1}'$ phase transforms discontinuously into Pc, which is a polar subgroup of $P2_1'/c$.

difference in the associated magnetoelectric coefficients. In addition, some form of spin-orbit coupling between the spin and orbital part of the toroidal moment would be expected, and the biquadratic product is the simplest symmetry-allowed way to achieve it. A remarkable property of this connection in $LiFeSi_2O_6$ is its extreme sensitivity to applied magnetic fields, attested, e.g., by the deactivation and decoupling of T^y from $T^{x,z}$ in a magnetic field H^y down to the resolution limit of the experiment. Such sensitivity is in agreement with the low symmetry of the magnetic phase. The triclinic symmetry does not impose restrictions on the orientation of the magnetic moments in three-dimensional space. Hence, a vanishingly small magnetic field can be sufficient to set the equilibrium direction of the magnetic moments and of the parameters derived from their arrangement (such as the toroidal moment) along a specific direction.

VI. PRIMARY FERROTOROIDICITY VERSUS PRIMARY ANTIFERROMAGNETISM

A central point of this work is the question whether a toroidal-free model can provide an equivalent interpretation of the observed magnetoelectric effects in $LiFeSi_2O_6$ via an exclusive coupling between the antiferromagnetic spin-density-wave order parameters spanned by the magnetic modes (L_1^x, L_3^y, L_1^z) and (L_3^x, L_1^y, L_3^z) which, as discussed, represent the same symmetries as T^y and $T^{x,z}$, respectively. In terms of *symmetry*, the required biquadratic coupling between the two antiferromagnetic order parameters is the sum of biquadratic products between their respective magnetic modes, i.e., $(L_1^x)^2(L_3^x)^2 + (L_1^x)^2(L_1^y)^2 + (L_1^x)^2(L_3^z)^2 + (L_3^y)^2(L_3^x)^2 + \cdots$. In terms of *physics*, their dominating contributions are those representing the exchange interaction between the localized spins. This is expressed by $(\mathbf{L}_1 \cdot \mathbf{L}_3)^2$, as the other terms represent relativistic interactions (e.g., spin-spin or spin-orbit) which are orders of magnitude smaller [18]. As depicted in Fig. 1(c), $\mathbf{L}_1$ and $\mathbf{L}_3$ are approximately perpendicular to each other. Therefore, the scalar product $\mathbf{L}_1 \cdot \mathbf{L}_3$ and the corresponding free-energy exchange contribution $\propto(\mathbf{L}_1 \cdot \mathbf{L}_3)^2$ are "geometrically attenuated" by the arrangement of the magnetic moments, an attenuation that does not apply to the toroidal moment. Thus, a triggering mechanism based on an antiferromagnetic order parameter seems highly unlikely in comparison to a triggering mechanism based on a toroidal order parameter. Instead, as depicted in the phase diagram of Fig. 5(b), a *two-step transition* to the triclinic phase is expected if the antiferromagnetic spin-wave order parameter is the primary one. In contrast, the *solitary transition* observed experimentally in $LiFeSi_2O_6$ points to a pronounced triggering mechanism and, hence, to a primary toroidal order parameter.

VII. CONCLUSION

In summary, our measurement of the linear magnetoelectric effect reveals that $LiFeSi_2O_6$ is a system where the macroscopic toroidal moment $\mathbf{T}$ instead of the antiferromagnetic vector $\mathbf{L}_{1,3}$ acts as the primary order parameter. This identification is based on physical microscopy and symmetry arguments: For both the toroidal-moment vector and the antiferromagnetic spin-wave vector, symmetry permits free-energy contributions with a biquadratic coupling of the respective vector components. Only the toroidal coupling term, however, can be large enough to drive a triggering mechanism with the simultaneous condensation of two irreducible order parameters, $\Gamma_1^- + \Gamma_2^-$, leading from the paramagnetic phase $P2_1/c1'$ to the experimentally observed triclinic phase $P\bar{1}'$ in a single step.

Note that primary ferrotoroidicity in antiferromagnets has been discussed before. In Ni-Cl, Co-I, and Co-Br boracites, a sharp anomaly of the linear magnetoelectric coefficient α_{zy} was associated to a toroidal order parameter [21,22]. The association to an equally possible antiferromagnetic order parameter was not discussed, though. Therefore, the distinction which is the very topic of our work has not been made and claims for primary ferrotoroidicity are yet to be justified. Reports on the observation of ferrotoroidic domains [4] and ferrotoroidic hysteretic switching [5] of a toroidal-moment vector in $LiCoPO_4$ did not extend to the question whether the toroidal order parameter is primary or induced. A distinction between ferrotoroidic and antiferromagnetic domains that was originally made for this system was later given up [1,5]. Additional measurements are also needed for confirming the primary toroidal origin proposed for the unusual critical behavior of the magnetic-field induced polarization in $Ba_2CoGe_2O_6$ [23].

Various potential primary ferrotoroidic compounds remain to be investigated. In particular the low-temperature sequences of weak-ferromagnetic polar phases found in Ni-Cl and Ni-Br boracites [24], or the specific features disclosed in the antiferromagnetic phase of $LiCrGe_2O_6$ [25], suggest that these materials could display a similar coupling between toroidal moment vector components as described for $LiFeSi_2O_6$ in the present work.

ACKNOWLEDGMENTS

The authors thank the Sinergia program of the Swiss National Science Foundation (Grant No. CRSII2_147606/1) for financial support and Nicola Spaldin for valuable discussion. M.F. and P.T. thank ETH Zürich for supporting P.T.'s stay as guest professor. The work in Cologne was supported by the Deutsche Forschungsgemeinschaft via SFB 608 and through the Institutional Strategy of the University of Cologne within the German Excellence Initiative.

[1] N. A. Spaldin, M. Fiebig, and M. Mostovoy, The toroidal moment in condensed-matter physics and its relation to the magnetoelectric effect, J. Phys.: Condens. Mat. **20**, 434203 (2008).

[2] C. Ederer and N. A. Spaldin, Towards a microscopic theory of toroidal moments in bulk periodic crystals, Phys. Rev. B **76**, 214404 (2007).

[3] B. Mettout, P. Tolédano, and M. Fiebig, Symmetry replication and toroidic effects in the multiferroic pyroxene $NaFeSi_2O_6$, Phys. Rev. B **81**, 214417 (2010).

[4] B. B. Van Aken, J.-P. Rivera, H. Schmid, and M. Fiebig, Observation of ferrotoroidic domains, Nature (London) **449**, 702 (2007).

[5] A. Zimmermann, D. Meier, and M. Fiebig, Ferroic nature of magnetic toroidal order, Nat. Commun. **5**, 4796 (2014).

[6] V. Dubovik and V. Tugushev, Toroid moments in electrodynamics and solid-state physics, Phys. Rep. **187**, 145 (1990).

[7] H. Schmid, Some symmetry aspects of ferroics and single-phase multiferroics, J. Phys.: Condens. Matter **20**, 434201 (2008).

[8] S. Jodlauk, P. Becker, J. Mydosh, D. Khomskii, T. Lorenz, S. Streltsov, D. Hezel, and L. Bohatý, Pyroxenes: A new class of multiferroics, J. Phys.: Condens. Matter **19**, 432201 (2007).

[9] S. Jodlauk, Neue Magnetoelektrika und magnetoelektrische Multiferroika, Ph.D. thesis, Universität zu Köln, Germany, 2010.

[10] G. Redhammer, G. Roth, W. Treutmann, M. Hoelzel, W. Paulus, G. André, C. Pietzonka, and G. Amthauer, The magnetic structure of clinopyroxene-type $LiFeGe_2O_6$ and revised data on multiferroic $LiFeSi_2O_6$, J. Solid State Chem. **182**, 2374 (2009).

[11] G. Redhammer, G. Roth, W. Paulus, G. André, W. Lottermoser, G. Amthauer, W. Treutmann, and B. Koppelhuber-Bitschnau, The crystal and magnetic structure of Li-aegirine $LiFe^{3+}Si_2O_6$: A temperature-dependent study, Phys. Chem. Minerals **28**, 337 (2001).

[12] M. Baum, Neutron-scattering studies on chiral multiferroics, Ph.D. thesis, Universität zu Köln, Germany, 2013.

[13] R. R. Birss, *Symmetry and Magnetism* (North-Holland, Amsterdam, 1966).

[14] M. Ackermann, Thermodynamic properties of new multiferroic and linear magnetoelectric crystals, Ph.D. thesis, Universität zu Köln, Germany, 2014.

[15] E. E. Wahlstrom, *Optical Crystallography* (Wiley, New York, 1960).

[16] H. Stokes and D. Hatch, *Isotropy Subgroups of the 230 Crystallographic Space Groups* (World Scientific, Singapore, 1988).

[17] G. Ljubarski, *Anwendungen der Gruppentheorie in der Physik* (VEB Deutscher Verlag der Wissenschaften, Berlin, 1962).

[18] I. Dzyaloshinskii, Theory of helicoidal structures in antiferromagnets. I. Nonmetals, J. Exptl. Theoret. Phys. (U.S.S.R.) **46**, 1420 (1964) [Sov. Phys. JETP **19**, 960 (1964)]; The theory of helicoidal structures in antiferromagnets. II. Metals, J. Exptl. Theoret. Phys. (U.S.S.R.) **47**, 336 (1964) [Sov. Phys. JETP **20**, 223 (1965)]; Theory of helicoidal structures in antiferromagnets. III., J. Exptl. Theoret. Phys. (U.S.S.R.) **47**, 992 (1964) [Sov. Phys. JETP **20**, 665 (1965)]; Thermodynamic theory of weak ferromagnetism in antiferromagnetic substances, J. Exptl. Theoret. Phys. (U.S.S.R.) **32**, 1547 (1957) [Sov. Phys. JETP **5**, 1259 (1957)].

[19] J. Holakovsky, A new type of the ferroelectric phase transition, Phys. Stat. Sol. **56**, 615 (1973).

[20] Y. Gufan and E. Larin, Theory of phase transitions described by two order parameters, Fiz. Tverd. Tela (Leningrad) **22**, 463 (1980) [Sov. Phys. Solid State **22**, 270 (1980)].

[21] D. Sannikov, Phenomenological theory of the magnetoelectric effect in some boracites, J. Exp. Theor. Phys. **84**, 293 (1997).

[22] D. Sannikov, Ferrotoroidic phase transition in boracites, Ferroelectrics **219**, 177 (1998).

[23] P. Tolédano, D. D. Khalyavin, and L. C. Chapon, Spontaneous toroidal moment and field-induced magnetotoroidic effects in $Ba_2CoGe_2O_7$, Phys. Rev. B **84**, 094421 (2011).

[24] P. Tolédano, H. Schmid, M. Clin, and J.-P. Rivera, Theory of the low-temperature phases in boracites: Latent antiferromagnetism, weak ferromagnetism, and improper magnetostructural couplings, Phys. Rev. B **32**, 6006 (1985).

[25] G. Nénert, M. Isobe, I. Kim, C. Ritter, C. V. Colin, A. N. Vasiliev, K. H. Kim, and Y. Ueda, Interplay between low dimensionality and magnetic frustration in the magnetoelectric pyroxenes $LiCrX_2O_6$ (X = Ge, Si), Phys. Rev. B **82**, 024429 (2010).